Journal of Membrane Science & Research

journal homepage: www.msrjournal.com

Research Paper

Molecular Dynamics Simulation of Gas Permeability Through Polyvinyl Acetate Membrane

Asma Sharififar [1], Omid Bakhtiari [1, 2, *], Behrouz Bayati [3]

[1] *Membrane Research Center, Faculty of Petroleum and Chemical Engineering, Razi University, Kermanshah, Iran.*
[2] *Membrane Research Center, Advanced Research Center for Chemical Engineering, Faculty of Petroleum and Chemical Engineering, Razi University, Kermanshah, Iran.*
[3] *Chemical Engineering Department, Faculty of Engineering, Ilam University, Ilam, Iran.*

Article info

Received 2023-01-13
Revised 2023-03-15
Accepted 2023-04-15
Available online 2023-04-15

Keywords

Membrane
Gas Separation
Permeability
Simulation
Molecular Dynamic
Grand Canonical Monte Carlo

Highlights

- Molecular Dynamics and Grand Canonical Monte Carlo simulation techniques were used.
- 42.82 Å cubic building blocks of the polyvinyl acetate (PVAc) were constructed.
- Constructed blocks by 30 vinyl acetate monomers have a density of 1.12 ± 0.02 g/cm^3.
- O_2, N_2, and CO_2 permeabilities through the PVAc membrane were satisfactorily determined.
- Results revealed higher penetrants solubility in PVAc membrane at higher pressures.

Graphical abstract

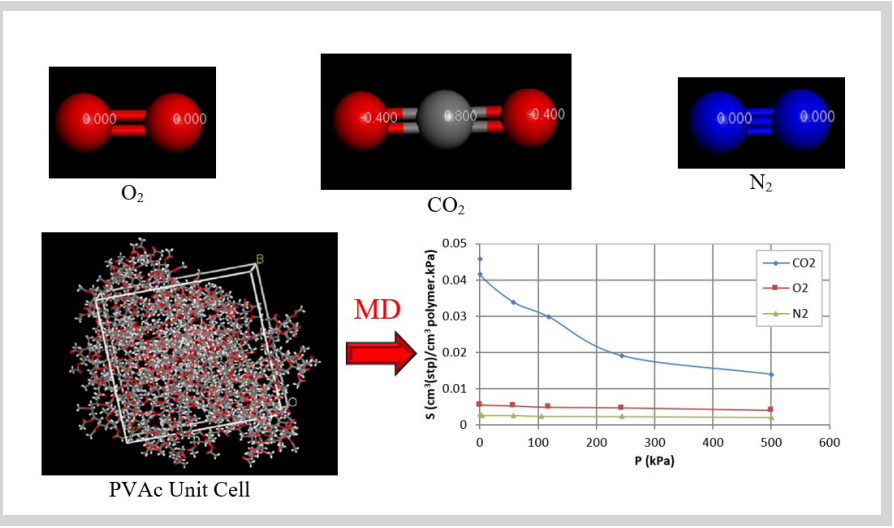

Abstract

Molecular Dynamics (MD) is an operative and powerful tool for forecasting of structural and performance characteristics of membranes. In the current research, the simulation techniques of MD and Grand Canonical Monte Carlo (GCMC) were used to predict diffusivities, solubilities, and permeabilities of gaseous penetrants of oxygen (O_2), nitrogen (N_2), and carbon dioxide (CO_2) through a tiny cell of polyvinyl acetate (PVAc) membrane. Diffusion coefficients of the penetrants were predicted via the NVT ensemble of MD simulation employing the condensed-phase optimized molecular potentials for atomistic simulation studies (COMPASS) force field up to a simulation time of 500 ps and their solubilities were predicted by employing the GCMC method. Then accordingly, the CO_2, N_2, and O_2 penetrants' permeabilities through the PVAc membrane were calculated as 4.661, 0.304, and 0.034 Barrer. The MD simulated permeabilities showed 9.8, 35.3, and 52.1 % of relative errors, respectively, as compared with the experimentally measured ones. The simulated results reveal acceptable accuracies.

1. Introduction

Carbon dioxide is produced in different fuels' combustion for supplying different energy demands and also in the manufacturing processes. Some CO_2 is also formed in chemical manufacturing as a side product, while almost is generated through different fossil fuels' combustion. One reason for global warming is large quantities of CO_2 emission which necessitates investigation for more energy-efficient processes for the separation/capture of CO_2 [1]. Membrane separation processes are appealing for CO_2 removal due to some advantages of this technology [2, 3]: at first, it requires no separating agent and separation does involve no phase changes. In addition, membrane processes require low maintenance and have small footprints compared to the other process. Membranes are light in weight and can be utilized as a multi-stage operation [1]. Membrane processes are also attractive selections for CO_2 removal/capture due to their improving intrinsic separation properties of this gas. CO_2 molecules are small and have a smaller kinetic diameter of 3.3 Å rather compared with those of other light gases like O_2 (3.46 Å) and N_2 (3.64 Å) [4]. Nowadays, polymeric membranes are attractive selections for gas separation arose of their easy processability and versatile modular forms, low initial and maintenance costs, footprints, and environmental impacts [5]. The

* Corresponding author: obakhtiari@razi.ac.ir (O. Bakhtiari)

DOI: 10.22079/JMSR.2023.1987383.1582

first polymeric commercial membrane was cellulose acetate which was prepared for the accompanying natural gas's CO_2 separation. After that, Monsanto introduced the first commercial air separation membrane as PRISM in 1980 [5]. In the late 1980s, some other manufacturers like Natco (Cynara), UOP (Separex), and Kvaerner (Grace Membrane Systems) were producing membrane units for the applications. After that, the cellulose acetate membrane was gradually replaced by polyimides and polyaramide ones, with higher selectivities, for CO_2 removal [1].

To date, polymers are the main employed materials for membrane preparation as pristine polymeric or as mixed matrix membranes. Membranes with glass transition temperatures (T_g) higher than their operating temperatures are glassy and those that operate at temperatures higher than their T_gs are rubbery polymers. Most commercial gas separations membranes are made of glassy polymers due to their great mechanical properties [6]. Common glassy polymers include polysulfones [7, 8], polyimides [9], polyamides and polycarbonates [10], polyphenylene oxides [11], polyvinyl acetate [12], and cellulose derivatives [7]. Nowadays, gas separation by glassy polymeric membranes remained a considerably attractive material as the literature survey reveals [13].

There is a tight relation between the polymeric membranes' structural properties and their separation performance. Some computer-based simulation software such as molecular simulations have been developed and enable researchers to quantitatively and qualitatively investigate the atomic/molecular level mechanisms that affect the behavior of polymeric materials (i.e., membranes). Also, they can utilize these computer calculations to predict the polymeric membranes' structural and transport properties with high accuracy [14].

The experimental investigation of the gaseous performance of the pristine polymeric and particles filled membranes are time and money-consuming and then some theoretical techniques were developed to simulate different parameters' effect on the membrane separation performance [15, 16]. Nowadays, computational calculations have been improved. The simulations of Molecular Dynamics (MD) and Monte Carlo (MC) are very attended methods to estimate gaseous penetrants' transport properties including their diffusivities, solubilities, and permeabilities through the polymeric membranes via strong virtual Labs [17,18]. By considering the presumption of conforming motion of the atoms by the laws of Newton and evaluation of their interactions by utilizing the experiential potential functions, MD is a very good tool to simulate different processes at the microscopic levels [19, 20]. Recently, molecular modeling (MM) obtain the ability to simulate and predict the membranes' structural and separation properties [21, 23].

For instance, Tung et al. using MD simulated the solvent type's effects on the atactic poly (methyl methacrylate)s (a-PMMA) membranes' total and available free fractional volume (FFV) and dynamic conformation of its matrix's polymer chains. They also evaluated the size distribution of the free volume in the PMMA membrane prepared by various solvents. They employed Grand Canonical Monte Carlo (GCMC) method to obtain the oxygen and nitrogen solubilities in the constructing material of the membrane. Simulation results showed that the penetrants' diffusion coefficient in the membrane is substantially determined by its free volume and fractional available volume and on the other hand the penetrants' solubility is affected by the free volume's size distribution at the interface [24]. Zhou et al. studied the penetration of different gaseous penetrants like nonhydrocarbons of H_2, O_2, N_2, and CO_2 and hydrocarbons of CH_4 and n-C_4H_{10} through the pristine and silica particles filled poly(1-trimethylsilyl-1-propyne, PTMSP) membranes utilizing MD NVT simulation techniques. They estimated gas diffusion coefficients by using the condensed-phase optimized molecular potentials for atomistic simulation studies (COMPASS) force field in simulation times of 500 and 1000 ps. Effects of the silica particle' loading and size on the penetrants' diffusivities, the membranes' free volume change, translational dynamics, and intermolecular energies were also investigated. The results revealed that the silica particles' incorporation into the PTMSP matrix increases the penetrants' diffusivities via an increment in the membrane matrix's free volume. They reported an n-butane diffusion coefficient of 3×10^{-5} cm^2/s at 60 wt. % of the filler particles loading [25]. Azizi and Mousavi applied MD and GCMC simulations to investigate diffusivities, solubilities, and permeabilities of the gaseous penetrants of CO_2, CO, H_2, and H_2O at different operation temperatures in a polyurethane (PU) membrane. The results showed that all the gas permeation was enhanced by increasing temperature from 298 to 318 K while their selectivities for CO_2/H_2 decreased. The CO_2 permeabilities through the membrane were found as 328.12, 494.15, and 777.12 in 298, 308, and 318 K [26].

Raghu et al. investigated the solubility parameters for PU membranes by using the MD method and found them in the range of 15.76 - 20.57 $(J/cm^3)^{0.5}$. The obtained solubilities were well in agreement with those of experimentally measured values, i.e., 2 - 3 % standard errors [27]. Rahmati et al. evaluated the polymerization degree's impacts on the structural and physical properties and also the separation performance of PU membranes by applying configuration bias MD and GCMC methods. They also evaluated the effects of the feed condition and the PU membranes' density and free volume on their separation performance. Their result indicated that water and furfural adsorption rates in the membrane increase by decreasing density and increasing PU's FFV [28]. Hu et al. studied diffusivities and sorption capacities (i.e., solubility) of the CO_2 and CH_4 in coal using MD and GCMC simulations. Their results revealed an acceptable prediction accuracy of the experimentally measured data as the estimated diffusion coefficient of CH_4 was found as 1.2×10^{-9} m^2/s vs. its experimental value of 1.02×10^{-9} m^2/s [15]. Dehghani et al. studied the structural and separation performance of polyether block amide (Pebax)-MFI nanozeolite mixed matrix membranes (MMMs) using the tools of molecular simulation (MS) and Monte Carlo (MC). They evaluated the MMMs microstructure, density, Radial Distribution Function (RDF), FFV and XRD pattern impacts on the solubilities and diffusivities of CO_2/CH_4 and CO_2/N_2 gas pairs. They also the effects of the MFI nanostructure and loading in the MMMs on their separation performance for natural gases, i.e. mixtures of CO_2, CH_4, and N_2, treatment. Their observations revealed that as the MFI nanozeolite loading in the MMMs increased from 10 to 20 wt. %, permeabilities of CO_2, CH_4, and N_2 increase from 106.5, 4.75, and 1.28 to 123.6, 4.74, and 1.31, respectively. Diffusivities of the CO_2, N_2, and CH_4 through the pure Pebax membrane were predicted as 0.043 (absolute relative error (ARE) of 5.5 %), 0.004, and 0.017 (R.E. of 4.8 %) cm^2/s, respectively. The CO_2, N_2, and CH_4 solubility through the pure polyether block amide membrane was predicted as 1.29, 0.114, and 0.324 cm^2/s which reveal AREs of 3.2, 47, and 8.0 %, respectively. Also, simulated structural analysis using MS and MC indicated very good agreement with results experimentally observed from the XRD patterns and also those measured for the penetrants' diffusivities [29].

The literature survey showed that there is no reported molecular simulation on the separation properties of gaseous penetrants through the polyvinyl acetate (PVAc) membrane. The principal goal of the current research is to estimate the transport properties of the PVAc membrane for CO_2, O_2, and N_2 penetrants using the MD and GCMC simulations. The PVAc density was estimated to investigate the applied model's accuracy and after the model's validation, the gaseous penetrants' diffusivities, solubilities, and permeabilities through the PVAc membrane were estimated.

2. Theory

Computer-based molecular simulation tools enable their users to understand the structural and microscopic interactions of atoms/molecules assemblies. They are basic/complementary concepts to the traditional experimental measurements and allow one to study new aspects of the phenomena that weren't understood in other ways. MS connects the microscopic phenomenon and time scales and those observed at the macroscopic level in the real-world/Labs: it provides estimations of the atoms/molecules intra/interactions and accordingly gives acceptable predictions in accuracy for the atoms/molecules constructed material's bulk characteristics. Obviously, MS predictions' accuracies compared with those of experimentally measured ones depend on the available hardware's configuration. Computer simulations can be carried out but sometimes they are hard or impractical to do in labs or large scales, i.e., limitations in providing very high or very low temperatures/pressures [30].

MD and GCMC are the two major class of simulation tools, to investigate the gas penetration through polymeric membranes. At first, the gaseous penetrants' diffusivities and solubilities should be estimated, and after that their permeabilities. Then, their permeabilities can be estimated by the solution-diffusion mechanism using the following equation:

$$P = D \times S \tag{1}$$

where P, D, and S are the penetrants' permeability usually reported in Barrer (1 Barrer = 10^{-10} cm^3 (STP) cm/cm^2.s.cm Hg), diffusion coefficient (cm^2/s), and solubility (cm^3 (STP)/cm^3 polymer.cm Hg). The diffusion coefficient corresponds to the dynamic behavior of the system of the penetrant-polymer and solubility indicates thermodynamic aspects of the penetrant-polymer mutual interactions [31].

2.1. Diffusion Prediction

For a non-equilibrated system, the system constituent particles diffuse from their initial places with high chemical/electrical/physical potentials to points that have lower potentials according to the motion equation. The mean square particles' movement from their initial location determines their second (and next) locations at later times (i.e., $t > 0$) [32]. In MD calculations, the

means of the Einstein relationship can be used for evaluating the moving atoms' diffusion coefficient (D) as follows [33, 34]:

$$D = \frac{1}{6N}\lim_{+\to\infty}\frac{d}{dt}\sum_{t=1}^{N}\langle|r_i(t)-r_i(0)|^2\rangle \quad (2)$$

which N is the diffusing atoms count, $r_i(t)$ and $r_i(o)$ indicate the i^{th} atom's position vector at time $t = t$ and the start time ($t = 0$) of movement, respectively, and the curly brackets state the mean square displacement (MSD)'s group average of the i^{th} atom entered and moves in a dynamics diffusion path. In order to predict the diffusion coefficient of an atom/molecule/particle in the Brownian (random) three-dimensional motion path, the MSD limiting slope vs. time is used. There are two typical regions for MSD, e.g., short and long times. In a short time the penetrating particle hits a tiny cavity of the membrane's free volume and is limited to it with no diffusion due to the short scale of time which accordingly, MSD remains constant. However, at the longer time scale, due to gradient potential across the membrane, the penetrant jumps out of its tiny cavity to the next and next lower potential cavities, i.e., the phenomenon of diffusion which is considered as linear MSD over time as described by Eq. 2. To obtain the penetrant's diffusivity, a straight line, i.e., $y = ax + b$, is fitted on the data of transport occurred by diffusion and the line's gradient of an in $Å^2/ps$ is extracted. According to the above definitions, D can be calculated as follows:

$$D = a/6 \quad (3)$$

MS software provides a graph of MSD over time and the best-fitted linear trend. As the line gradient, i.e. a is obtained, it is divided by 6 to convert to the penetrant's coefficient of diffusion in $Å^2/ps$ which can be further divided by 10^{-4} to convert it to the common unit of cm^2/s) [32].

2.2. Solubility Prediction

The GCMC method can be utilized in the simulation process in order to evaluate the gas solubility coefficient. The method was based on the penetrant gaseous molecule(s) concentration probability as its energy changes the previous configuration to the new one to receive or discard a configurational movement of a penetrant's molecule according to the Metropolis algorithm [24]. The Metropolis Monte Carlo algorithm can be applied to investigate the adsorbate molecules' adsorption with no interior degree of freedom in porous frameworks. The algorithm tries just the locations and alignments of the adsorbate molecules and each conformation is considered an inflexible frame. The Metropolis algorithm is usually considered for adsorbate molecules with a smaller size compared with the pore sizes diffusing through in a such manner there is no considerable torsional flexibility [32].

In order to simulate gas molecules' absorption in their transport through a membrane, the adsorbate molecules' locations could be created and destroyed transitionally and rotationally in a random manner. A penetrated gas molecule randomly dislocates in all directions of x, y, or z during its transfer across the membrane and its transitional movement with an acceptance probability (P_{acc}) is evaluated as follows [24, 28]:

$$P_{acc}(Old \to New) = \min\left[1, \exp(-\Delta E / K_B T\right] \quad (4)$$

where ΔE may be evaluated in terms of the non-bonded potentials of van der Waals and Coulombic interactions as a measure of the adsorbate molecule's energy change from the old configuration to the new one, K_B is the Boltzmann constant and T is the absolute temperature of penetration in K. van der Waals and Coulombic forces (or static electricity) among atoms are two main terms of their non-bonded potentials:

$$E_{non-bonded} = E_{van-der-Waals} + E_{Coulombic} \quad (5)$$

In the van der Waals potential term, all the atoms (even those that have no net electrostatic charge) tend to attract each other from a far distance to a specific close distance as described by the attractive negative term. As the atoms get near enough and their electron clouds are overlapped, the repulsive positive term of the potential becomes more and more determined that finally repels them from each other. A famously employed function for the van der Waals 6 - 9 potential is the simple Lennard - Jones expression with acceptable accuracy [35]:

$$\sum_{VdW} E = \sum_{ij}\varepsilon_{ij}\left[2\left(\frac{\sigma_{ij}}{r_{ij}}\right)^9 - 3\left(\frac{\sigma_{ij}}{r_{ij}}\right)^6\right] \quad (6)$$

$$\sigma_{ij} = \left(\left(\sigma_i^6 + \sigma_j^6\right)/2\right)^{1/6} \quad (7)$$

$$\varepsilon_{ij} = 2\sqrt{\varepsilon_i \varepsilon_j}\,\frac{\sigma_i^6 \sigma_j^6}{\sigma_i^6 + \sigma_j^6} \quad (8)$$

where r_{ij} is the i and j atoms' center-to-center distance, $\sigma_i\sigma_j$ and $\varepsilon_i\varepsilon_j$ are stand for size and energy terms for atoms i and j. Opposite electrostatic charges appeal while the same charges deny each other. The Coulombic force ($E_{Coulombic}$) interactions can be estimated using the method of Ewald [35]:

$$E_{Coulombic} = \sum_{ij}\frac{q_i q_j}{r_{ij}} \quad (9)$$

where q_i and q_j are the electrical charges of the atoms i and j, respectively. The energy term of non-bonded can be evaluated within a cut-off distance of the r_{ij}. As the cut-off distance is more than that between atom i and atom j, the non-bonded energies of the van der Waals and Coulombic force may be evaluated by their associated potential functions [24].

Adsorbate molecules are randomly embedded in the membrane cell for the rotational movement and also an axis is also randomly selected for this type of movement where the adsorbate molecule accidentally rotates around it. According to the change in energy, the next configuration was considered for translational movement with the same probability as stated by Eq. 4. The acceptance probability of move creation and destruction for gas species are given by Eqs. 11 and 12, respectively [24, 28]:

$$P_{acc}(Old \to New) = \min\left[1, \exp\left(-\frac{\Delta E}{K_B T} - \ln\left[\left(\left(N_i + 1\right)K_B T\right)/\left(f_i V\right)\right]\right)\right] \quad (10)$$

$$P_{acc}(Old \to New) = \min\left[1, \exp\left(-\frac{\Delta E}{K_B T} \pm \ln\left[\left(N_i K_B T\right)/\left(f_i V\right)\right]\right)\right] \quad (11)$$

where f_i is the gas phase fugacity of the i^{th} specie, V is the volume of the membrane cell and N_i is the species count of the i^{th} component in this volume. The i^{th} species solubility may be evaluated in the form of a simulated plot of its concentration against pressure (or fugacity) range of 0 - 1 atm at a constant temperature [36, 37]. Adsorbate gas molecules concentration is procurable by the overall probability of 1 million steps. The gradient of the concentration-pressure plot as the pressure approaches zero is usually utilized to evaluate adsorbate gas solubility (S in $cm^3(STP)/cm^3\ polymer.cm\ Hg$) by following equation [38]:

$$S = \lim_{p\to 0}\left(\frac{C}{p}\right) \quad (12)$$

where C is the sorbate concentration in $cm^3(STP)/cm^3\ polymer$, and p is the pressure in cm Hg.

3. Simulation Details

In MS, each atom's distance (r), charge (q), bond angles, and momentum (m + v) information is defined and used for all the dissolving molecules. MD simulation carries out by stepwise numerical solution of the motion as described by the second law of Newton at the atomic level [30]:

$$m_i \ddot{r}_i = F_i, \quad F_i = -\frac{\partial V}{\partial r_i} \quad (13)$$

where m_i and $\ddot{r}_i$ are the i^{th} atom's mass and motion acceleration, respectively, F_i is the acting force on the i^{th} atom in the potential energy of V. For this purpose, acting force(s), F_i, on the atoms is typically obtained from the potential energy of V(r^N), where $r^N = (r_1, r_2, \ldots, r_N)$ represents 3 N atomic coordinates [30]. One of the most important factors in MD simulation is the selection of proper force field(s) in strength to access reliable results as compared with the experimentally measured ones. The COMPASS force field can control the motion of all the atoms in the simulated membrane cell [39, 40]. A typical atom could be affected by the potential energy functions of all the other atoms present in the simulated system, namely bonded (E_{bonded}) and non-bonded ($E_{non-bonded}$) potential energies, as given by the following equation:

$$V(R) = E_{bonded} + E_{non-bonded} \quad (14)$$

For molecular structures, the interactions of intramolecular bonding should also be considered. The simplest molecular model contains the following terms:

$$E_{bonded} = E_{bond-stretch} + E_{angle-bend} + E_{\varphi} \quad (15)$$

where $E_{bond-stretch}$, $E_{angle-bend}$, and E_{φ} are two adjacent atoms' bond stretching placed in an amorphous cell, the atom's bond angle's rotation degree, and the torsional angle deviations, respectively. In the COMPASS force field, $E_{bond-stretch}$ is usually described by the quartic potential function energy as follows [41]:

$$E_{bond-stretch} = \sum_{i=2}^{4} k_i (b - b_0)^i \quad (16)$$

where k_i's are constants for force and b_0 and b is the equilibrium and dynamic lengths of a bond. Both k_i's and b_0 were calculated using quantum mechanics or semi-empirical correlations. The bond angle's rotation degree (i.e., three-atom movement) can be calculated from the quartic potential function of θ values [41]:

$$E_{angle-bend} = \sum_{i=2}^{4} H_i (\theta - \theta_0)^i \quad (17)$$

where H_i's are force constants, and θ and θ_0 are dynamic and equilibrium bond angles. The changes of torsional angle (dihedral angle, or four adjacent atoms movement) are usually calculated from the θ quartic potential function, i.e., Fourier expansion function, as described by the following equation:

$$E_{\varphi} = \sum \left\{ V_1 \left[1 - \cos(\varphi - \varphi_1^0) \right] + V_2 \left[1 - \cos(2\varphi - \varphi_2^0) \right] + V_3 \left[1 - \cos(3\varphi - \varphi_3^0) \right] \right\} \quad (18)$$

where V_i's are the force constants, and φ and φ_i's are dynamic and the equilibrium torsional angles of the polymer chains [30].

3.1. Amorphous Cell Construction

In the current research, the solubilities, diffusivities, and permeabilities of the gaseous penetrant of O_2, N_2, and CO_2 through pristine polyvinyl acetate were simulated by utilizing MD and MC simulations. At first, the vinyl acetate monomer and then PVAc polymer chains with 30 monomers were constructed by using the Build module in the material studio software, version 4.3. Then, its energy was minimized by the Discover module and smart minimizer with 10,000 irritations. The molecular structure of the PVAc chain and that of simulated PVAc chains in the current study are presented in Fig. 1 and Fig. 2, respectively.

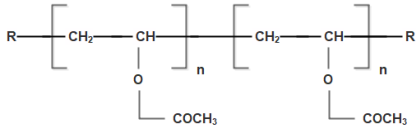

Fig. 1: The chemical structure of the PVAc chain.

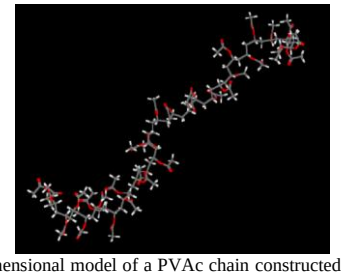

Fig. 2: The three-dimensional model of a PVAc chain constructed in the material studio software.

To construct an amorphous cell, as a small part of the membrane, 15 PVAc chains (each one constructed with 30 monomers) were inserted in a cell, as is shown in Fig. 3, and ten independent configurations under periodic boundary condition (PBCs) of 303 K and initial density of 0.1 g/cm^3 were examined based on the Odoreou and Suter method using the software's Amorphous Cell Module [42]. Since small densities may lead to continuous system fluctuation, it is necessary to select proper initial densities to eventually access an acceptable density close to that of practical packing value [43]. In addition, low densities cause keeping the simulated system from catenation and spearing of the polymer chains.

In the current simulation and as can be observed in Fig. 3, some parts of the PVAc chains are indwelled outdoors the boundaries of the simulated cell. PBCs are considered as those reported by Allen [30] and Leach [44].

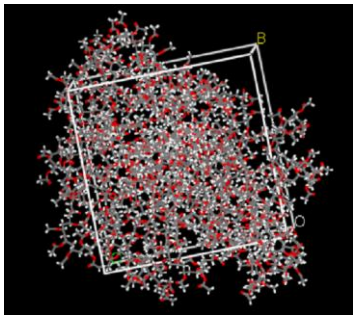

Fig. 3: The optimized PVAc chains in the simulated amorphous cell as a part of the PVAc membrane.

3.2. Energy Minimization

During the simulation procedure, constructed atomic structure energy should be minimized which was performed by the smart minimizer method (SMM) as an element of the Discover module. In SMM, the COMPASS force field is applied to minimize cell energy in order to remove all the closed contacts. The SMM employs the Conjugate Gradient method to minimize the energy of the molecular structure of the polymeric chains. PVAc's total potential and non-bound energies as the function of time-step are presented in Fig. 4. As it is revealed, the PVAc total energy decreased from - 11500 to - 13900 kCal.mol^{-1} after 2000 iterations and reached its final approximated value indicating the system energy has been minimized truly [45].

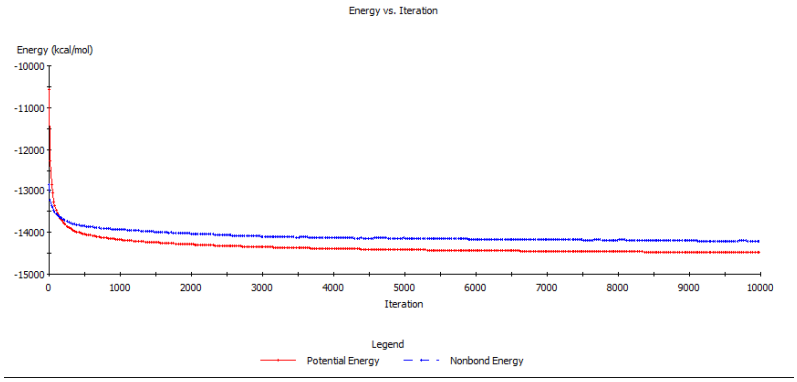

Fig. 4: Potential energy and non-bond energy graph during energy minimization.

3.3. Equilibrium Step

An ideal structure is defined as a structure with the lowest energy level and as much as similar to the actual one. After minimization and to access the ideal molecular structure, NPT (fixed atoms number, temperature, and pressure) runs were performed at constant atoms number, temperature, and pressure, and time-step of 5430 atoms, 303 K, 800 kPa, and 1 fs, respectively. The methods of Anderson and Berendsen were used, respectively, as the thermostat and the barostat for controlling temperature and pressure [28, 46]. Through all the simulation runs, the algorithm of the velocity Verlet was employed for integration of the equation of Newton's second law with a 1 fs time step. Electrostatic intermolecular forces were determined with 0.001 kCal.mol^{-1} by the Ewald method [14]. In this study, 12.5 Å of distance cutoff was considered in the 6 - 9 function of the Lenard-Jones type potential for taking into account intermolecular forces of the Van der Waals type. The distance cutoff was lower than the half length of the simulated membrane cell at 42.82 Å.

As the procedures of minimization and optimization (their data are provided in the supplementary information as Fig.s S1 to S5) were finished, the relaxed structure (as is shown in Fig. 3) with the equilibrium cell density and length of approximately 1.12 ± 0.01 g/cm^3 and 42.82 Å were obtained. The experimental density of PVAc was reported as 1.18 g/cm^3, revealing acceptable accuracy [12].

3.4. Gas Molecules Embedding for Diffusivity Simulation

To evaluate the diffusivity coefficient of studied gases, it is necessary to insert gaseous molecules into the equilibrated configurations as discussed in section 2.1. The gas molecules' energies were minimized initially by the Discover module, then 6 molecules of each penetrant of N_2, O_2, and CO_2 were inserted into the cell in separate steps by performing Locate task in the Sorption module.

Each cell was filled by PVAc polymer chains and gas molecules. To relax the cell, it should reach an equilibrium state, due to the executed NPT and NVT steps for the time of 500 ps. At the end of the NVT run, the diffusivity coefficient was calculated by the Forcite module and the determination of MSD [45].

3.5. Simulation of Penetrants Solubility

The solubilities of the gaseous penetrants' molecules were evaluated by employing the sorption module, the adsorption isotherm task [47], and the method of Metropolis [40]. The pressure range for this simulation was 0 - 5 atm where the sorption isotherms were predicted. The starting equilibration period was set to one hundred thousand steps and at every pressure, one million steps of GCMC calculations were carried out.

4. Results and Discussions

4.1. Predicted Diffusion Coefficient of Gaseous Penetrants

Routes of the gas molecules penetrating in PVAc membrane in a 500 ps period of NVT for MD simulation runs are shown in Fig. 5. As can be observed, a gas molecule vacillates in a peculiar void and as the polymer chain creates a proper route, it irregularly jumps into a next adjacent void. These outlines of the gas molecules' routes approve the usual hopping mechanism of molecules penetration in the polymer matrix. Also, it can be obviously understood that the CO_2 molecules jump longer than the O_2 and N_2 molecules, dedicating them to higher permeabilities.

The studied gaseous molecules' diffusivities were estimated by the initial gradient of their associated MSD-time graphs and the diffusivities are reported in Table 1. As is observed in Fig. 5, there is a rise after a while, the energy of the gas molecules increased after a short simulation time via the impact of polymer chains atoms on their vibrational movements. Hence, the penetrants' molecules obtain sufficient energy to jump to an adjacent cavity that has enough space to hold them. According to this description, it appears that CO_2 and O_2 molecules gain higher energies for longer jumps. The magnitude of diffusivity of the studied gases is $CO_2 > O_2 > N_2$. Two factors influence the diffusion coefficient's magnitude: the penetrating molecules' dimension and the structural and morphological properties of the polymer [48]. To evaluate the size effect of the studied penetrants molecules on their diffusivities, their volume and surface area of van der Waals was obtained by Connolly surface and are reported in Table 1.

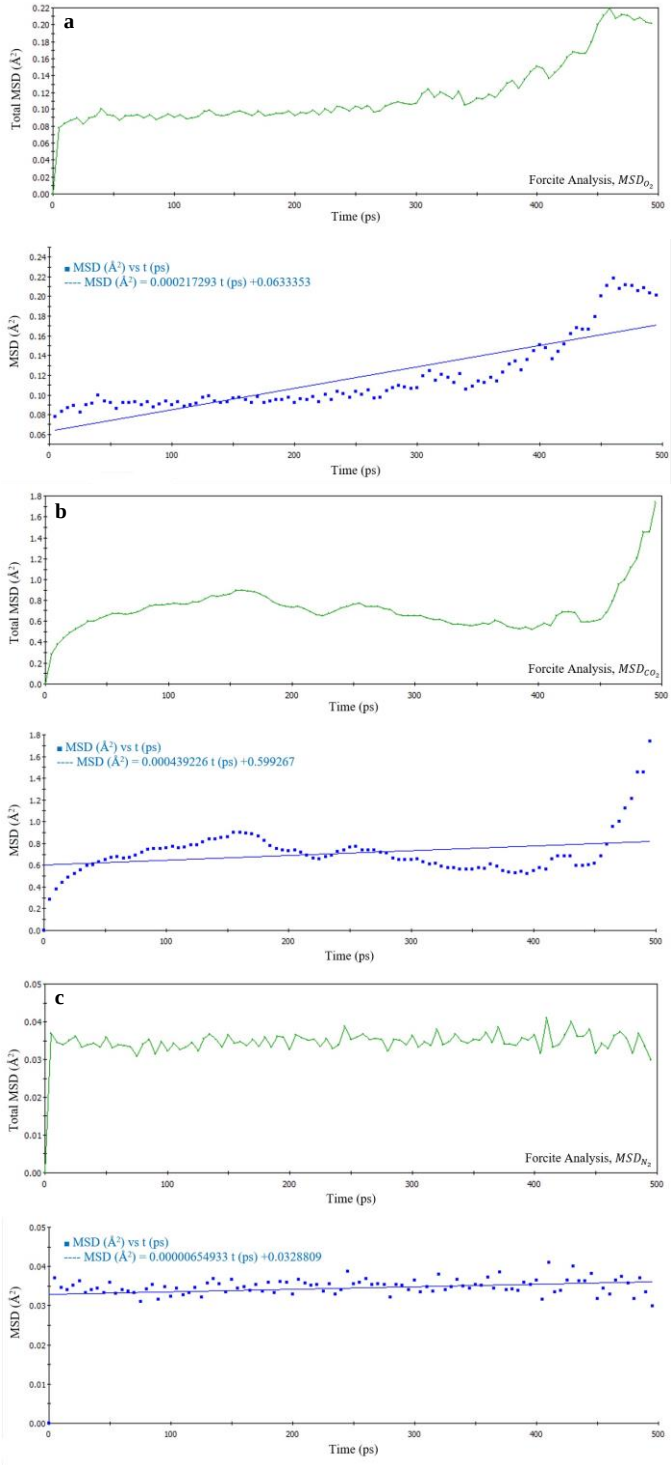

Fig. 5: MSD - time graphs of the penetrants of a) O_2, b) CO_2, and c) N_2.

Table 1
Molecular properties size of the studied gaseous penetrants.

Gaseous penetrant	van der Waals Volume (Å^3)	Surface area (Å^2)	Kinetic diameter (Å)	Diffusivity coefficient (× 10^9 cm^2/s)
CO_2	33.58	50.28	3.30	7.3167
O_2	24.44	40.87	3.46	3.6167
N_2	23.37	38.66	3.64	1.0134

Taking into account the penetrant molecular size, it is expected that the diffusion coefficient of the smallest molecule to be greater than the other molecules, however, the calculated diffusion coefficients show otherwise. For

instance, the O_2 molecule's van der Waals volume and surface area are greater than those of the N_2 molecule while the results showed that the O_2 diffusion coefficient is greater than that of N_2. This outcome reveals that there should be another factor, which is kinetic diameter that contributes to determining the impact on the gaseous penetrant's diffusion coefficients. The smallest effective size of a gaseous molecule is kinetic diameter which depends on the molecular spatial structure and also has to determine the effect on its transport [49]. O_2 kinetic diameter is smaller than that of N_2 which can be attributed to its more compact electron cloud around O nuclei in each molecule. This compactness is due to the existence of more robust electrostatic interactions between the negative charges of the electrons and positive charges of O atoms' nuclei in the O_2 molecule. Then, the magnitude of the penetrants' diffusivities is proportional to the reverse of their kinetic diameters (as reported in Table 1). ln(D) of the penetrants vs. their kinetic diameters are shown in Fig. 6 which reveals confirms those penetrants have smaller kinetic diameters that have higher diffusivities [49].

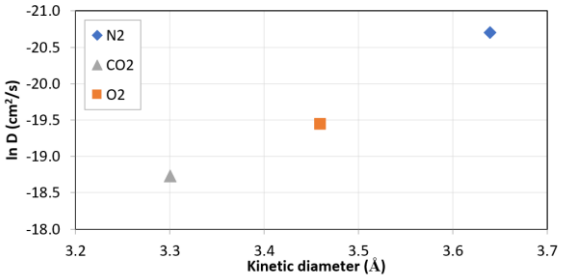

Fig. 6: Calculated diffusion coefficients of gaseous penetrants vs. their kinetic diameters.

The gaseous penetrants' diffusivities in the polymeric membranes are less than 10^{-5} cm^2/s [50], whereas those of Knudsen diffusion are around 10^{-3} cm^2/s. The calculated diffusivities in the current study are less than 10^{-5} cm^2/s and it can be understood that diffusion in the PVAc is according to molecular diffusion as stated based on the solution-diffusion mechanism solution-diffusion.

4.2. Predicted Solubilities of Gaseous Penetrants

The pure gases of O_2, N_2, and CO_2 loading per unit cell of PVAc membrane were investigated at 303 K and in 0 - 5 atm by the GCMC ensemble with the Metropolis method [15, 28] and the results are revealed in Fig. 7. Then, accordingly, the penetrant concentrations in the PVAc membrane were calculated and the outcomes are shown in Fig. 8. Finally, the solubilities of the penetrants were estimated by Eq. 12 and their values are reported in Table 2.

Table 2
Predicted gaseous penetrants' solubilities in the current study.

Gaseous Penetrant	Solubility (cm^3 (STP)/cm^3 polymer.atm)	Diffusivity (10^9 cm^2/s)
CO_2	4.8414	7.3167
O_2	0.5266	3.6167
N_2	0.2575	1.0134

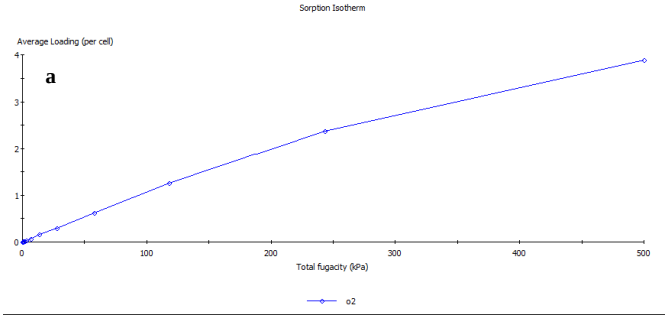

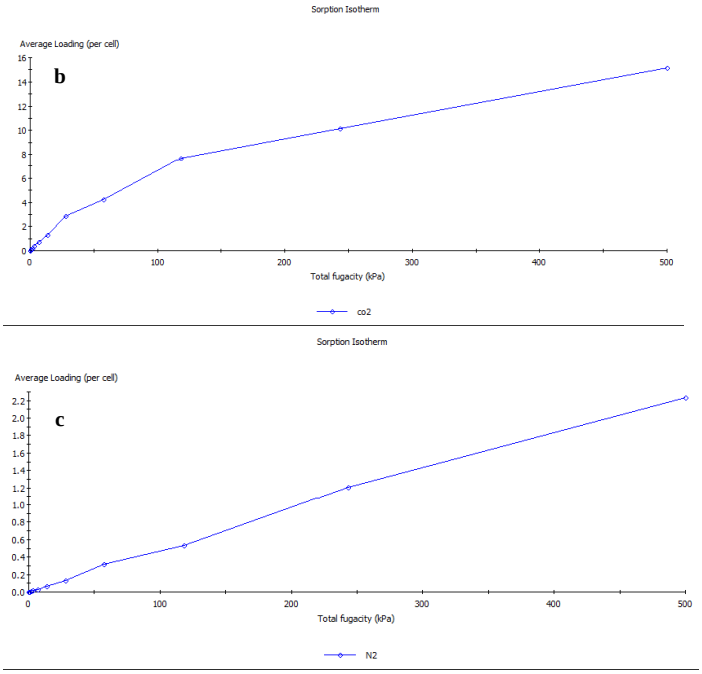

Fig. 7: Predicted adsorption isotherms of a) O_2, b) CO_2, and c) N_2.

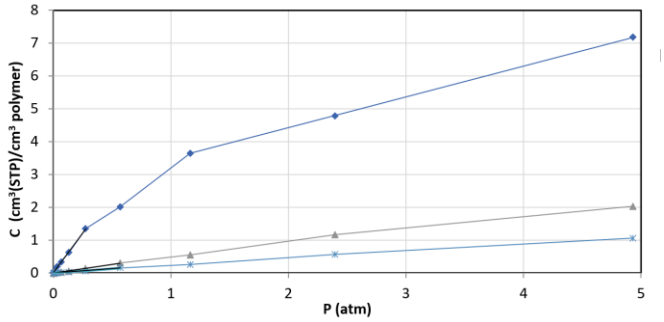

Fig. 8: The predicted solubilities of CO_2, O_2, and N_2 adsorbed molecules loading onto the PVAc membrane at 303 K and 0 - 5 atm.

As is observed, at high gas pressures the concentration of the gaseous penetrants in the polymer matrix increase. The initial increment rate of the gas concentrations at lower gas pressures is higher than those at higher gas pressure which can be due to the faster saturation rate of the available free volume of the polymer. Condensability and charge of the gas molecules are responsible for their solubilities. The obtained solubility magnitude of the gaseous molecules is $CO_2 > O_2 > N_2$ which is in agreement with that of their condensability consequence. Also, CO_2 is quadrupolar but N_2 and O_2 are nonpolar molecules and all these facts resulted in greater CO_2 solubility in the PVAc membrane than the other examined gases. A gas molecule's condensability depends on its critical temperature, as can be observed in Fig. 9, gaseous penetrants with higher critical temperatures have higher solubilities. Additionally, the energy distribution of N_2, O_2, and CO_2 molecules in the PVAc membrane was calculated to check the accuracy of the simulated results, and the results are shown in Fig. 10. Some peaks are shown and as can be observed in the energy value of CO_2 is greater than the other gases indicating CO_2 has a good affinity toward the PVAc membrane due to the greater interaction energy of CO_2 molecules with PVAc. Thereupon, the CO_2 solubility is higher than the other gases [51-53].

CO_2 has strong quadrupole moments (4.1×10^{-26} e.s.u) while O_2 and N_2 have no net charge and therefore it has stronger interactions with the PVAc polymeric chains. As a result, CO_2 molecules tend to be more adsorbed in the PVAc membrane than other gaseous penetrants and this effect reveals its high solubility. The interactions between gas molecules - polymer chains and the polymer's available free volume content and distribution [54] are important factors affecting gas solubility in polymers.

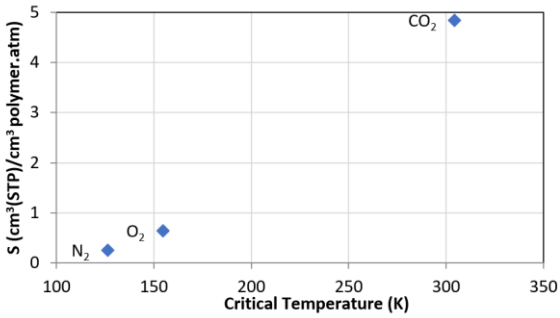

Fig. 9: Relationship between the gaseous penetrants' solubilities and their critical temperatures as a measure of their condensability.

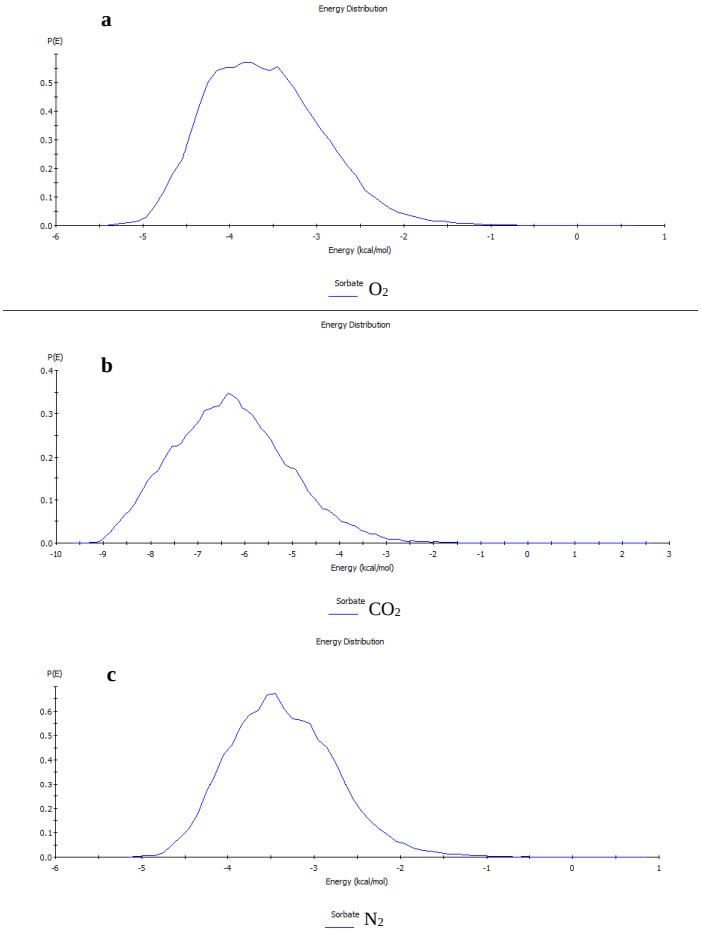

Fig. 10: Distribution of sorption energy of a) O_2, b) CO_2, and c) N_2 at 303 K and 0 - 1 atm.

To examine the accuracy of the simulated solubilities, the gaseous penetrants' adsorption behavior from low to high pressures was considered. The dual-mode sorption model, as described by Eqs.19 and 20, was used for the penetrants concentration in the membrane body [55]:

$$C = C_D + C_H = k_D p + \frac{C'_H bp}{1+bp'} \quad (19)$$

$$S \equiv \frac{C}{p} = S_D + S_H = k_D + \frac{C'_H b}{1+bp'} \quad (20)$$

where C, C_D, C_H are the total, Henry's law, Langmuir sorption concentrations in the glassy polymer, k_D is the coefficient of Henry's law, b and c'_H are the Langmuir isotherm's parameters, respectively, S is the gaseous penetrant's solubility, and S_D and S_H indicate solubilities as given by Henry's law and Langmuir isotherm, respectively. The k_D, c'_H, and b were estimated for N_2, O_2, and CO_2 and are reported in Table 3.

As can be observed in Fig. 11, both Henry's law and the Langmuir isotherm at lower pressure solubility values depend on the pressure. At the higher pressures, the solubility becomes nearly constant indicating the gaseous penetrants' solubility didn't depend on the applied pressure, as Henry's law states. The free volume of a typical glassy polymeric membrane can be categorized into two micro-void and free volumes created in inter-chains of the polymer macromolecules which respectively provide the sorption types of Langmuir and Henry's law. As is shown in Fig. 11, as the gas phase pressure increases, its solubility in the polymer decreases which reveals the sorption type of Langmuir at low-pressure regions as Eqs. 19 and 20 describe. At the lower pressures, gas molecules are captured easier by the membrane's micro-voids, while the gas molecules simultaneously have a tendency to locate close to the inter-molecular chains as symbolic of both sorption types of Langmuir and Henry's law. At higher pressures, the adsorption sites close to the micro-voids will gradually be saturated to vanish the sorption type of Langmuir and left Henry's sorption type as the remained model of adsorptions.

Fig. 11 reveals, among the studied gas species, N_2 sorption completely follows Henry's law due to the immediate filling of the membrane's micro-voids by the N_2 molecules at low pressures. The smaller N_2 molecules in size and critical temperature dedicated them lower affinity toward the PVAc membrane matrix and minor solubility compared with the other gas molecules. The CO_2 molecules with higher critical temperatures have a higher affinity toward the membrane and it is the cause of CO_2's high solubility. The sorption types' difference between Henry's law and the Langmuir isotherm for the CO_2 molecules are more considerable compared with the other two gas molecules as the applied pressure increases; i.e., this penetrant's solubility decreased dramatically at higher pressures.

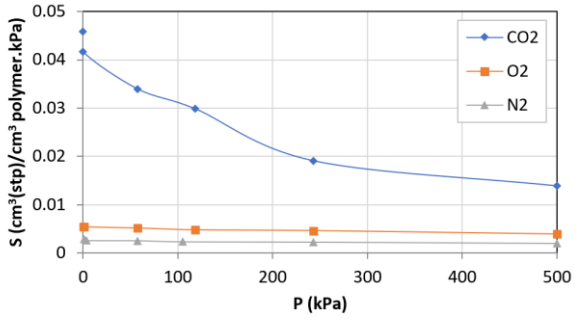

Fig. 11: Different gaseous penetrants' predicted solubilities versus pressure in the PVAc membrane at 303 K.

Table 3
Evaluated parameters of k_D, c'_H, and b for CO_2, O_2 and N_2 onto the PVAc membrane.

Penetrant	k_D (cm³ (STP)/cm³ polymer.cm Hg)	c'_H (cm³ (STP)/cm³ polymer)	b (cmHg^{-1})
CO_2	6.573×10^{-1}	4.599	1.138
O_2	-4.488×10^{-1}	34.349	2.861×10^{-2}
N_2	-3.594×10^{-2}	10.757	2.639×10^{-2}

4.3. Predicted Gaseous Penetrants Permeabilities through PVAc Membrane

The gaseous penetrants' permeabilities may be evaluated by the product of their predicted diffusivities and solubilities, Eq. 1 states. The predicted and experimental permeabilities of the studied gaseous permeabilities through the PVAc membrane and their relative absolute errors are reported in Table 4. As the results reveal, the highest CO_2 permeability can be attributed to its high solubility. CO_2 gas molecules have a great affinity toward the PVAc matrix due to its molecules' polarity and after CO_2, O_2 molecules have the next high permeability, and the lowest permeability was found for the N_2 molecules. However, the kinetic diameters of these molecules are in reverse order: $N_2 > O_2 > CO_2$. It can be concluded as the solution-diffusion mechanism states, the solubilities of the studied penetrants have higher impacts on their permeabilities through the PVAc membranes than their diffusivities [4]. The results reveal acceptable accuracies compared with those of experimentally measured results.

Table 4
The experimental and simulated gaseous permeabilities at 8 atm and 303 K and their corresponding absolute relative errors (ARE) for the PVAc membrane.

Gaseous penetrant	Permeability (Barrer)		
	Experimental	Simulated	ARE (%)
CO_2	5.17	4.661	9.8
O_2	0.47	0.251	46.5
N_2	0.071	0.034	52.1

5. Conclusion

MD simulation and Monte Carlo techniques were employed to investigate the transport properties of the gaseous penetrant including CO_2, O_2, and N_2 through the PVAc membrane. The aim was followed by the investigation of the gaseous penetrants' diffusion, solubility, and permeability of the membrane. The simulation outcomes revealed that the permeability of CO_2 is greater than O_2 and N_2, it can be concluded that the PVAc membrane is proper for CO_2 removal. The calculated permeabilities agree properly with those measured experimentally for the PVAc membrane revealing that the MS techniques are reliable enough for the prediction of the polymeric membranes' separation properties for gaseous penetrants. These methods also supply some insights into understanding the molecular configuration impacts on the structural designing and tailor-making of the polymeric membranes' separation performance.

Funding

No financial support was provided for this work.

CRedit authorship contribution statement

A. Sharififar: Data curation; Roles/Writing - original draft; Formal analysis.
O. Bakhtiari: Investigation; Methodology, Project administration; Resources; Supervision; Validation; Visualization; Writing – review & editing..
B. Bayati: Conceptualization; Validation; Visualization.

Declaration of Competing Interest

The authors declare that they have no known competing financial interests or personal relationships that could have appeared to influence the work reported in this paper.

References

[1] J. Ritter; A. Ebner, Carbon dioxide separation technology: R&D needs for the chemical and petrochemical industries. Chemical Industry Vision 2007, (2020) 287-295.
[2] R. W. Baker, Future Directions of Membrane Gas Separation Technology. Ind. & Eng. Chem. Res. 41 (2002) 1393-1411. https://doi.org/10.1021/ie0108088.
[3] M. Freemantle, Membranes for gas separation. Chem. Eng. News 83 (2005) , 49-57. https://doi.org/10.1021/cen-v083n040.p049.
[4] S. Matteucci, Y. Yampolskii;B. D. Freeman, I. Pinnau, Transport of Gases and Vapors in Glassy and Rubbery Polymers. In Materials Science of Membranes for Gas and Vapor Separation, John Wiley & Sons, Ltd, 2006; pp 1-47.
[5] R. Baker, J. Wijmans, J. Kaschemekat, The design of membrane vapor–gas separation systems. J. Membr. Sci. 151 (1998), 55-62. http://doi.org/10.1016/S0376-7388(98)00248-8.
[6] S. A. Stern, Polymers for gas separations: the next decade. J. Membr. Sci. 94 (1994), 1-65. http://doi.org/10.1016/0376-7388(94)00141-3.
[7] S.-H. Choi, M.-K. Lee, S.-J. Oh; J.-K. Koo , Gas sorption and transport of ozone-treated polysulfone. J. Membr. Sci. 221 (2003), 37-46. http://doi.org/10.1016/S0376-7388(03)00081-4.
[8] T.-S. Chung, J. J. Shieh, W. W. Y. Lau, M. P. Srinivasan, D. R. Paul , Fabrication of multi-layer composite hollow fiber membranes for gas separation. J. Membr. Sci. 152 (1999) 211-225. http://doi.org/10.1016/S0376-7388(98)00225-7.
[9] Shao, L.; Chung, T.-S.; Goh, S. H.; Pramoda, K. P. Transport properties of cross-linked polyimide membranes induced by different generations of diamino butane (DAB] dendrimers. J. Membr. Sci. 238 (2004) 153-163. http://doi.org/10.1016/j.memsci.2004.03.034.
[10] F. Hamad, K. Khulbe, T. Matsuura, Comparison of gas separation performance and morphology of homogeneous and composite PPO membranes. J. Membr. Sci. 256 (2005), 29-37. https://doi.org/10.1016/j.memsci.2004.12.050.
[11] S.-H. Chen, S.-L. Huang, K.-C. Yu, J.-Y. Lai, M.-T. Liang, Effect of CO_2 treated polycarbonate membranes on gas transport and sorption properties. J Meme Sci 172 (2000), 105-112. http://doi.org/10.1016/S0376-7388(00)00323-9.
[12] J. Ahmad, M.-B. Hägg , Preparation and characterization of polyvinyl acetate/zeolite 4A mixed matrix membrane for gas separation. J. Membr. Sci. 427 (2013) 73-84. http://doi.org/10.1016/j.memsci.2012.09.036.
[13] S. Banerje, G. Maier; C. Dannenberg, J. Springer, Gas permeabilities of novel poly (arylene ether)s with terphenyl unit in the main chain. J. Membr. Sci. 229 (2004), 63-71. https://doi.org/10.1016/j.memsci.2003.09.016.
[14] D. N. Theodorou, Principles of molecular simulation of gas transport in polymers. in materials science of membranes for gas and vapor separation, John Wiley & Sons, Ltd, 2006; pp 49-94.
[15] H. Hu, X. Li, Z. Fang, N. Wei, Q. Li, Small-molecule gas sorption and diffusion in coal: molecular simulation. Energy J 35 (2010), 2939-2944. https://doi.org/10.1016/j.energy.2010.03.028.
[16] Z. Zhou, J.-H. Cheng, T.-S. Chung, T. A. Hatton, The exploration of the reversed enantioselectivity of a chitosan functionalized cellulose acetate membrane in an electric field-driven process. J. Membr. Sci. 389 (2012) 372-379. http://doi.org/10.1016/j.memsci.2011.11.002.
[17] A. H. Haghighi, M. M. Hasani-Sadrabadi, E. Dashtimoghadam, G. Bahlakeh, S. E. Shakeri, F. S. Majedi, S. H. Emami, H. Moaddel, Direct methanol fuel cell performance of sulfonated poly (2, 6-dimethyl-1, 4-phenylene oxide)-polybenzimidazole blend proton exchange membranes. International journal of hydrogen energy 36 (2011), 3688-3696. https://doi.org/10.1016/j.ijhydene.2010.12.101.
[18] M.Sadeghi, M. A. Semsarzadeh, M. Barikani, B. Ghalei, Study on the morphology and gas permeation property of polyurethane membranes. J. Membr. Sci. 385-386 (2011) 76-85. http://doi.org/10.1016/j.memsci.2011.09.024.
[19] K.-S.Chang, Y.-H. Huang, K.-R. Lee, K.-L. Tung, Free volume and polymeric structure analyses of aromatic polyamide membranes: A molecular simulation and experimental study. J. Membr. Sci. 354 (2010) 93-100. http://doi.org/10.1016/j.memsci.2010.02.076.
[20] H.Ebro, Y. M. Kim, J. H. Kim, Molecular dynamics simulations in membrane-based water treatment processes: A systematic overview. J. Membr. Sci. 438 (2013) 112-125. http://doi.org/10.1016/j.memsci.2013.03.027.
[21] I. G. Economou, V. E. Raptis, V. S. Melissas, D. N. Theodorou, J. Petrou, J. H. Petropoulos, Molecular simulation of structure, thermodynamic and transport properties of polymeric membrane materials for hydrocarbon separation. Fluid Ph. Equilibria 228–229 (2005) 15-20. http://doi.org/10.1016/j.fluid.2004.08.026.
[22] S. S. Jawalkar, T. M. Aminabhavi, Molecular modeling simulations, and thermodynamic approaches to investigate compatibility/incompatibility of poly(l-lactide) and poly(vinyl alcohol) blends. Poly. J. 47 2006, (23), 8061-8071. http://doi.org/10.1016/j.polymer.2006.09.030.
[23] F. Pan, J. Ma, L. Cui, Z. Jiang, Water vapor/propylene sorption and diffusion behavior in PVA–P(AA-AMPS) blend membranes by GCMC and MD simulation. Chem. Eng. J. 64 (2009) 5192-5197. http://doi.org/10.1016/j.ces.2009.08.026.

[24] K.-L. Tung, K.-T. Lu, R.-C. Ruaan, J.-Y. Lai, MD and MC simulation analyses on the effect of solvent types on accessible free volume and gas sorption in PMMA membranes. Desalination 192 (2006) 391-400. https://doi.org/10.1016/j.desal.2005.08.018.
[25] J.-H. Zhou, R.-X. Zhu, J.-M. Zhou, M.-B. Chen, Molecular dynamics simulation of diffusion of gases in pure and silica-filled poly (1-trimethylsilyl-1-propyne)[PTMSP]. Polymer J. 47 (2006) 5206-5212. https://doi.org/10.1016/j.polymer.2006.05.041.
[26] M. Azizi, S. A. Mousavi, CO_2/H_2 separations using a highly permeable polyurethane membrane: Molecular dynamics simulation. J. Mol. Struct. 1100 (2015) 401-414. https://doi.org/10.1016/j.molstruc.2015.07.029.
[27] A.Raghu, G.Gadaginamath, S. Jawalkar, S. Halligudi, T. M. Aminabhavi, Synthesis, characterization, and molecular modeling studies of novel polyurethanes based on 2, 2′-[ethane-1, 2-diylbis (nitrilomethylylidene)] diphenol and 2, 2′-[hexane-1, 6-diylbis (nitrilomethylylidene)] diphenol hard segments. J. Polym. Sci. Part A: Polymer Chemistry, 44 (2006) 6032-6046. https://doi.org/10.1002/pola.21686.
[28] M. Rahmati, H. Modarress, R. Gooya, Molecular simulation study of polyurethane membranes. Polymer J., 53 (2012) 1939-1950. https://doi.org/10.1016/j.polymer.2012.02.051.
[29] M. Dehghani, M. Asghari, A. H. Mohammadi, M. Mokhtari, Molecular simulation and Monte Carlo study of structural-transport-properties of PEBA-MFI zeolite mixed matrix membranes for CO2, CH4, and N2 separation. Comput. Chem. Eng. 103 (2017) 12-22. https://doi.org/10.1016/j.compchemeng.2017.03.002.
[30] M. P. Allen, Introduction to molecular dynamics simulation. Computational soft matter: from synthetic polymers to proteins John von Neumann Institute for Computing, Julich, ¨ NIC Series, 23 (2004) 1-28. http://www.fz-juelich.de/nic-series/volume23.
[31] F. Mozaffari, H. Eslami, J. Moghadasi, Molecular dynamics simulation of diffusion and permeation of gases in polystyrene. Polymer J. 51 (2010) 300-307. http://doi.org/10.1016/j.polymer.2009.10.072.
[32] Biovia materials studio, an integrated, multi-scale modeling environment. Available on: https://www.3ds.com/products-services/biovia/products/molecular-modeling-simulation/biovia-materials-studio.
[33] N.Hu, J. R. Fried, The atomistic simulation of the gas permeability of poly(organophosphazenes). Part 2. Poly[bis(2,2,2-trifluoroethoxy)phosphazene]. Polymer J. 46 (2005) 4330-4343. http://doi.org/10.1016/j.polymer.2005.03.017.
[34] X.-Y. Wang, R. D. Raharjo, H. J. Lee, Y. Lu, B. D. Freeman, I. C. Sanchez, Molecular simulation and experimental study of substituted polyacetylenes: fractional free volume, cavity size distributions, and diffusion coefficients. J. Phys. Chem. B. 110, (2006), 12666-12672. https://doi.org/10.1021/jp060234q.
[35] J. Xu, W. Zhao, Y. Ning, M. Bashari, Z. Jin, B. Xu, L. Zhang, X. Duan, H.Chen, F. Wu, Can helical spring dextrin be composed of higher eight glucose units per turn? J. Mol. Struct. 1036 (2013) 274-278. http://doi.org/10.1016/j.molstruc.2012.11.064.
[36] Q. L. Liu, Y. Huang, Transport behavior of oxygen and nitrogen through organasilicon-containing polystyrenes by molecular simulation. J. Phys. Chem. B. 110 (2006) 17375-17382. https://doi.org/10.1021/jp063174x.
[37] J. Z. Yang, Q. L. Liu, H. T. Wang, Analyzing adsorption and diffusion behaviors of ethanol/water through silicalite membranes by molecular simulation. J. Membr. Sci., 291 (2007) 1-9. http://doi.org/10.1016/j.memsci.2006.12.025.
[38] J. R.; Fried, P. Ren, The atomistic simulation of the gas permeability of poly(organophosphazenes). Part 1. Poly(dibutoxyphosphazenes). Comput. Theor. Polym. Sci. 10 (2000) 447-463. http://doi.org/10.1016/S1089-3156(00)00005-2.
[39] M. P. Allen, D. J. Tildesley, Computer simulation of liquids; Oxford university press, 1989.
[40] N. Metropolis, A. W. Rosenbluth, M. N. Rosenbluth, A. H. Teller, E. Teller, Equation of state calculations by fast computing machines. J. Chem. Phys., 21 (1953) 1087-1092. https://doi.org/10.1063/1.1699114.
[41] J.-R. Hill, J. Sauer, Molecular mechanics potential for silica and zeolite catalysts based on ab initio calculations. 2. aluminosilicates. J. Chem. Phys., 99 (1995) 9536-9550. https://doi.org/10.1021/j100023a036.
[42] D. N. Theodorou, U. W. Suter, Detailed molecular structure of a vinyl polymer glass. Macromolecules, 18 (1985) 1467-1478. https://doi.org/10.1021/ma00149a018.
[43] M. Heuchel, D.Hofmann, Molecular modelling of polyimide membranes for gas separation. Desalination, 144 (2002), 67-72. https://doi.org/10.1016/S0011-9164(02)00290-4.
[44] Leach, A. R. Molecular modelling: principles and applications; Pearson Education, 2001.
[45] K. Golzar, S. Amjad-Iranagh, M. Amani, H. Modarress, Molecular simulation study of penetrant gas transport properties into the pure and nanosized silica particles filled polysulfone membranes. J. Membr. Sci. 451 (2014) 117-134. http://dx.doi.org/10.1016/j.memsci.2013.09.056.
[46] X.-Y. Wang, A. J. Hill, B. D. Freeman, I. C. Sanchez, Structural, sorption and transport characteristics of an ultrapermeable polymer. J. Membr. Sci., 314 (2008) 15-23. http://doi.org/10.1016/j.memsci.2007.12.074.
[47] N. Follain, J.-M. Valleton, L. Lebrun, B. Alexandre, P. Schaetzel, M. Metayer, S. Marais, Simulation of kinetic curves in mass transfer phenomena for a concentration-dependent diffusion coefficient in polymer membranes. J. Membr. Sci. 349 (2010) 195-207. http://doi.org/10.1016/j.memsci.2009.11.044.
[48] E. Földes, B. Turcsányi, Transport of small molecules in polyolefins. I. Diffusion of Irganox 1010 in polyethylene. J. Appl. Polym. Sci., 46 (1992) 507-515. https://doi.org/10.1002/app.1992.070460317.
[49] M. Amani, S. Amjad-Iranagh, K. Golzar, G. M. M. Sadeghi, H. Modarress, Study of nanostructure characterizations and gas separation properties of poly (urethane–urea)s membranes by molecular dynamics simulation. J. Membr. Sci. 2014, 462, 28-41. https://doi.org/10.1016/j.memsci.2014.03.018.
[50] A. Hill, B. D. Freeman, M. Jaffe, T. Merkel, I. Pinnau, Tailoring nanospace. J. Mol. Struct., 739 (2005), 173-178. https://doi.org/10.1016/j.molstruc.2004.05.041.
[51] Y. Liu, N. Li, X. Cui, W. Yan, J. Su, L. Jin, A Review on the morphology and material properties of the gas separation membrane: molecular simulation. Membranes 12 (2022) 1274. https://doi.org/10.3390/membranes12121274.
[52] M. Amani, S. Amjad-Iranagh, K. Golzar, G. M. M. Sadeghi, H. Modarress, Study of nanostructure characterizations and gas separation properties of poly(urethane–urea)s membranes by molecular dynamics simulation. J. Membr. Sci. 462 (2014) 28-41. https://doi.org/10.1016/j.memsci.2014.03.018.
[53] K. Asif, S. S. Lock, S. A. Taqvi, N. Jusoh, C. L. Yiin, B. L. Chin, A. C. Loy, A molecular simulation study of silica/polysulfone mixed matrix membrane for mixed gas separation. Polymers, 13 (2021) 2199. https://doi.org/10.3390/polym13132199.
[54] Y. Chen, Q. L. Liu, A. M. Zhu, Q. G. Zhang, J. Y. Wu, Molecular simulation of CO_2/CH_4 permeabilities in polyamide-imide isomers. J. Membr. Sci., 348 (2010) 204-212. http://doi.org/10.1016/j.memsci.2009.11.002.
[55] S. Kanehashi, K. Nagai, Analysis of dual-mode model parameters for gas sorption in glassy polymers. J. Membr. Sci. 253, (2005) 117-138. https://doi.org/10.1016/j.memsci.2005.01.003.

Supplementary Information

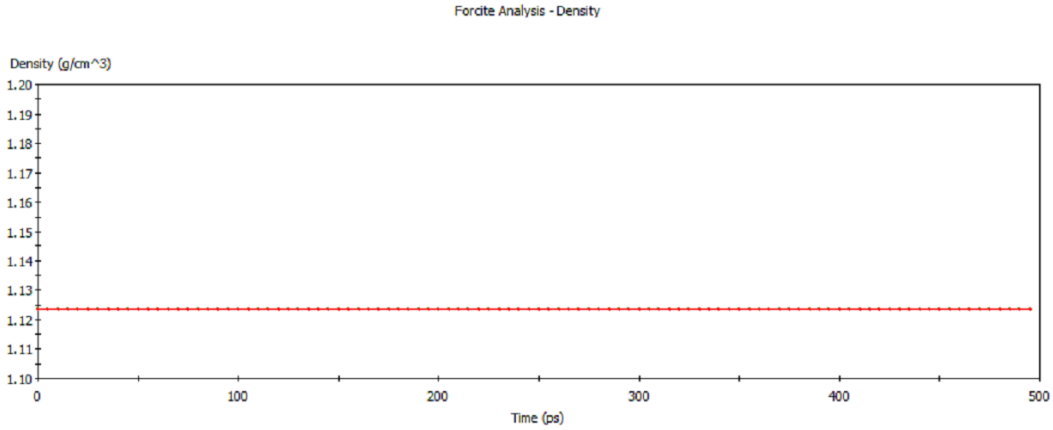

Fig. S1: Unit cell density over the minimization and optimization steps.

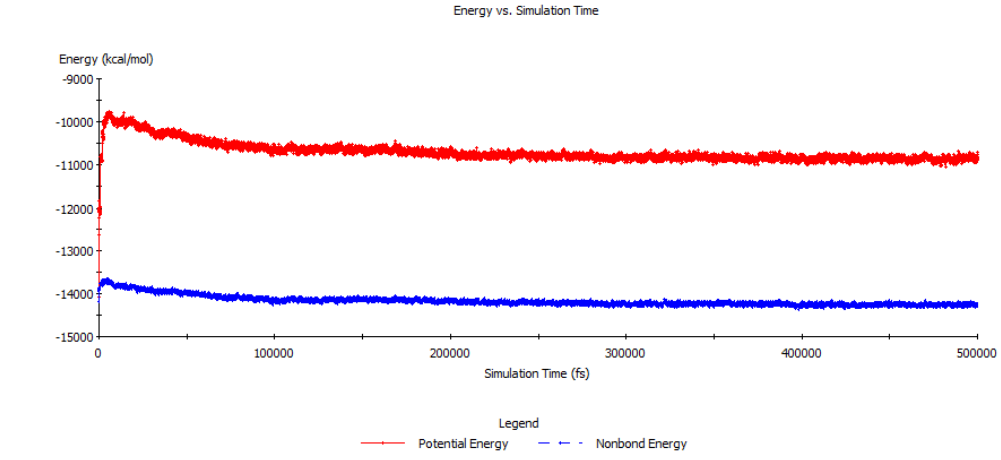

Fig. S2: Potential energy and non-bond energy versus time graph in NPT run.

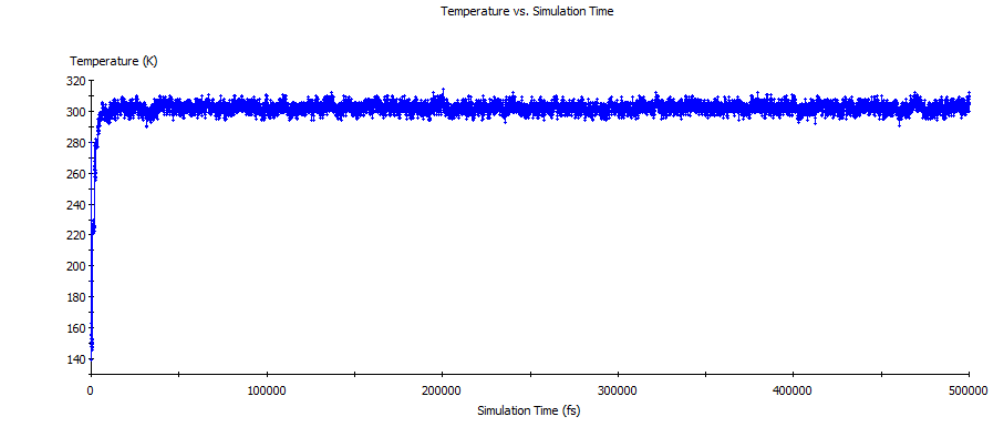

Fig. S3: Temperature versus time graph in NPT run.

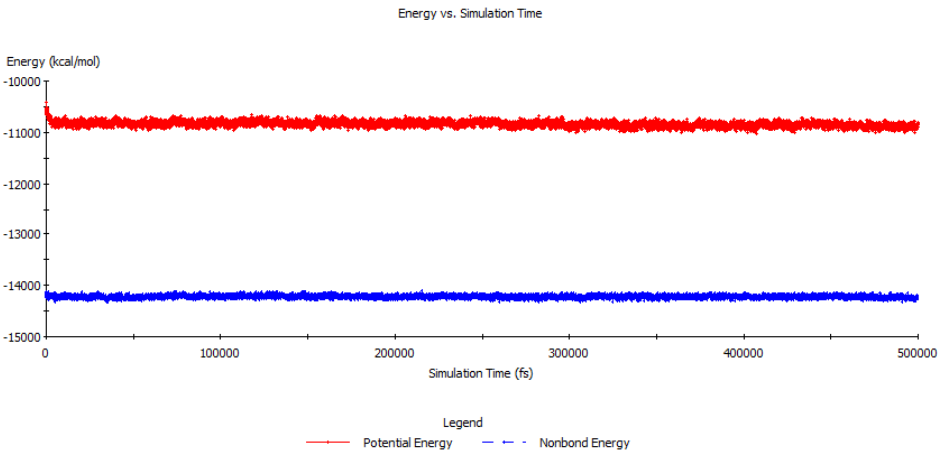

Fig. S4: Potential energy and non-bond energy versus time graph in NVT run.

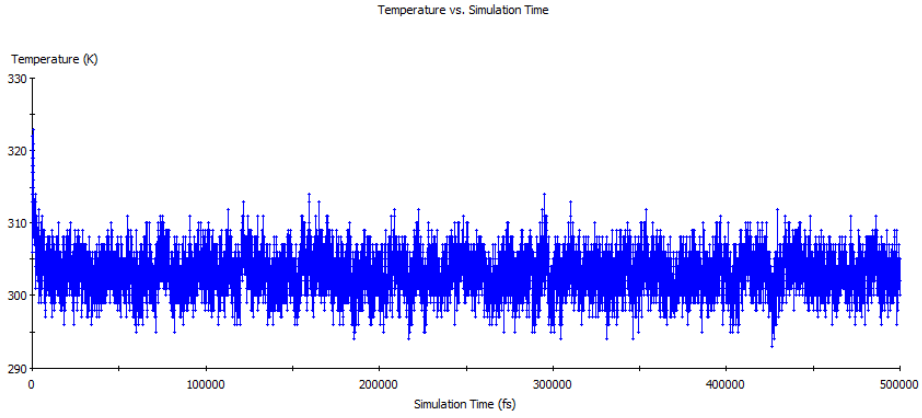

Fig. S5: Temperature versus time graph in NVT run.